Monte Carlo simulation of the neutron monitor yield function

Mangeard et al., Res. Space Physics 121, 7435 (2016)

Jclub

18/11/2016

1. Introduction: CRs + modulation + Rc + atmosphere

1. Transport in the Galaxy
→ Interstellar (IS) spectra

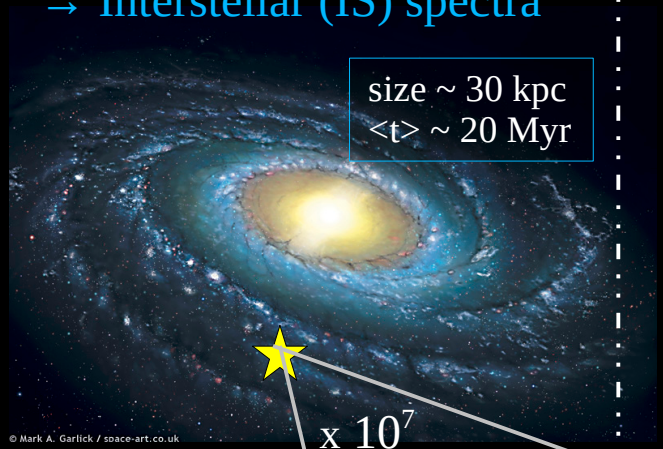

x 10^7

3. Earth magnetic shield
→ Cut-off rigidity R_c (at Earth)

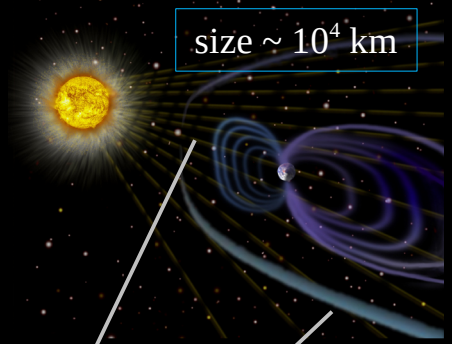

x 10^5

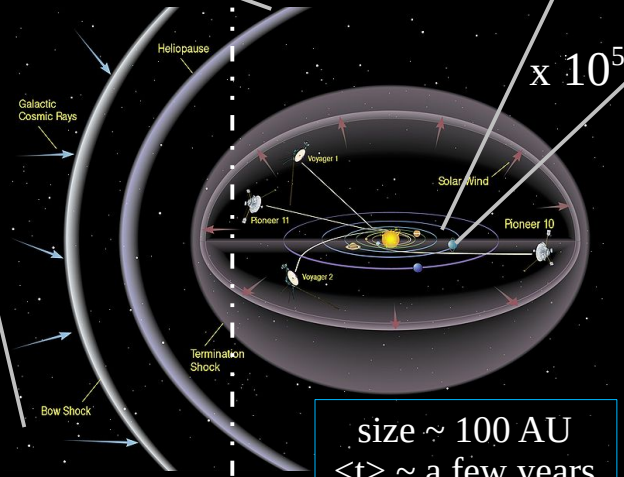

size ~ 100 AU
<t> ~ a few years

2. Transport in the Solar cavity
→ modulate CRs (< 10 GeV/n)

[time-independent]

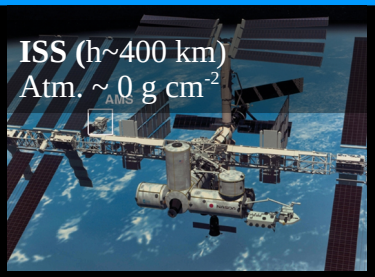

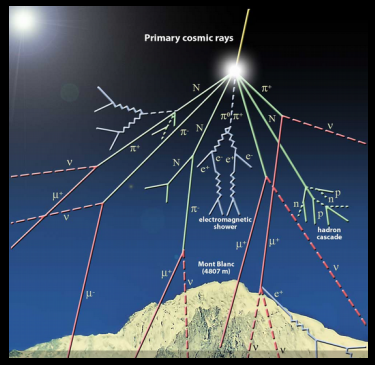

4. Atmosphere
→ CR showers
[time-dependent]

1. Introduction: IS fluxes, TOA fluxes, and count rates

1. Transport in the Galaxy
→ Interstellar (IS) spectra

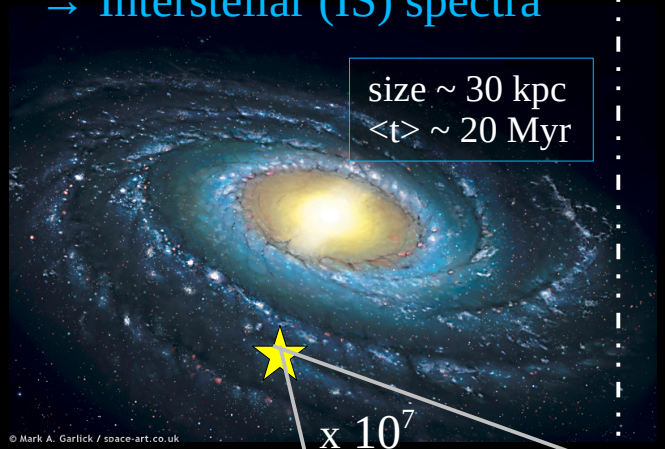

x 10^7

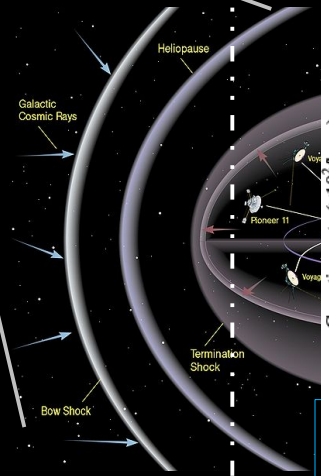

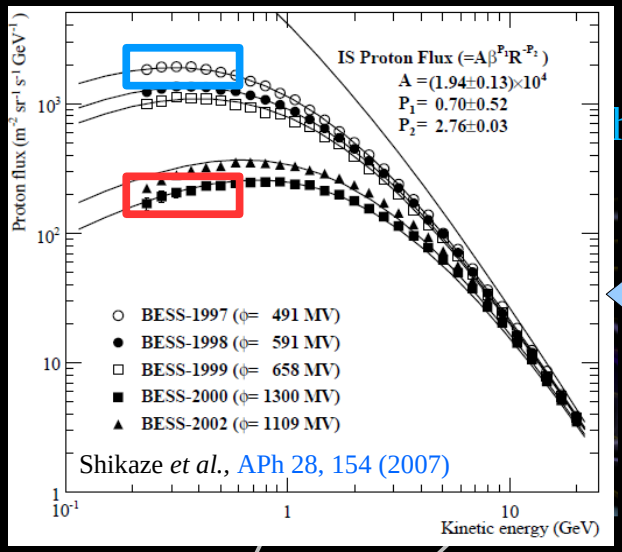

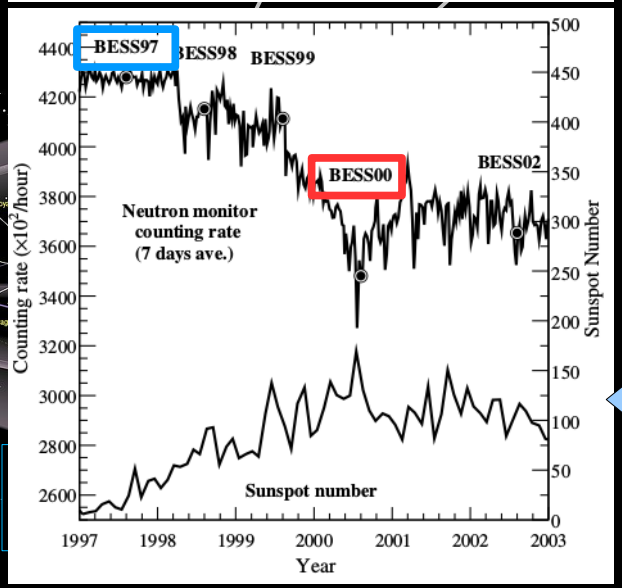

2. Transport in the Solar cavity
→ modulate CRs (< 10 GeV/n)

[time-independent]

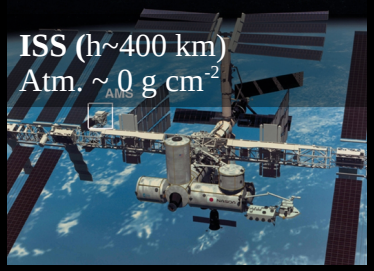

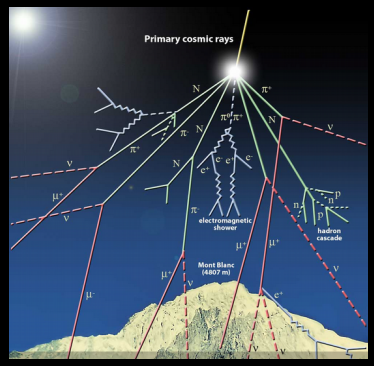

4. Atmosphere
→ CR showers
[time-dependent]

Les moniteurs à neutrons (NM)

(from A. Ghelfi)

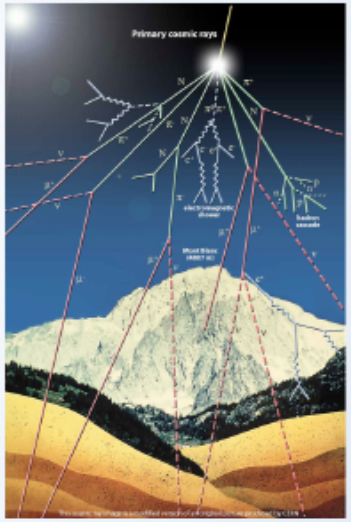

Détecteurs au sol sensibles aux neutrons produits dans les gerbes atmosphériques.

- Développés dans les années 50.
- Résolution temporelle ≈ 10 minutes.
- Signal intégré : mesure un taux de comptage.

Commonly used reactions: 3He(n,p) 3H, 6Li(n,α) 3H, 10B(n,α) 7Li

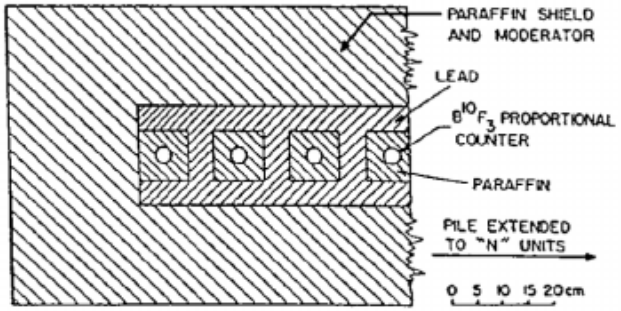

[Simpson 2000]

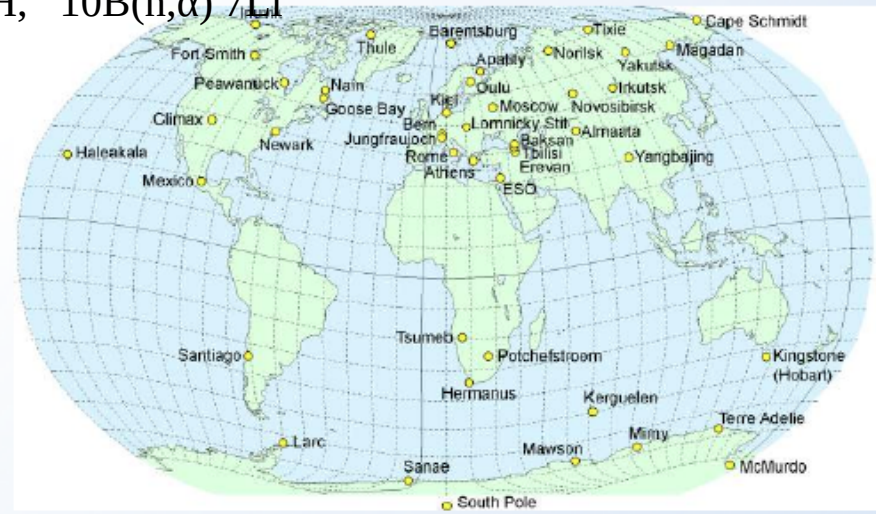

nmdb.eu

Détecteur simple, permet une observation continue depuis les années 50.

Les moniteurs à neutrons (NM)

(from A. Ghelfi)

Modélisation du signal attendu dans un NM [Dorman 2004] :

$$N(\vec{r},t) = k_{calib} \int_0^{\infty} T(R,\vec{r},t) \times \sum_{i=i_{CR}} Y_i(R,h)\, J^i_{TOA}(R,t)\, dR$$

Taux de comptage dans le NM.

Facteur de calibration (calculé à partir des expériences TOA).

Fonction de transmission du champ magnétique terrestre.

Fonction de *yield*. Modélise l'atmosphère terrestre et le NM.

Flux TOA. Dépend de J_{IS} et ϕ.

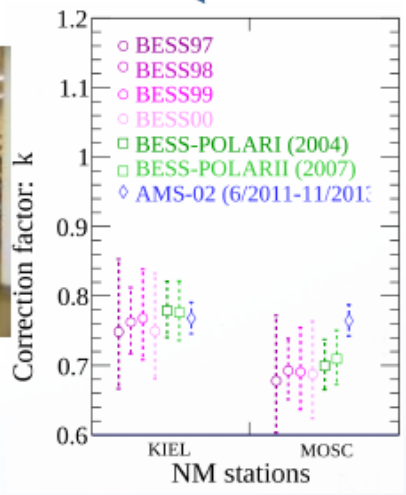

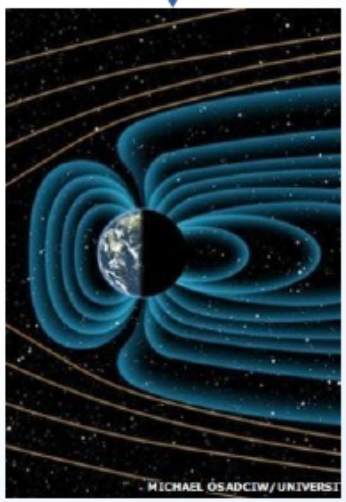

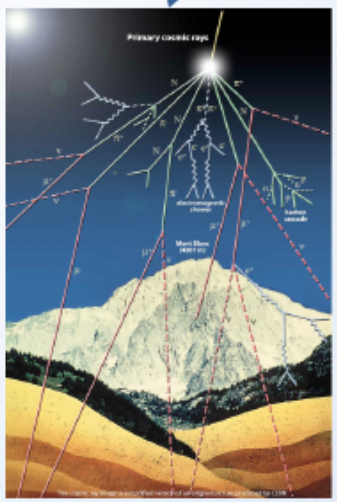

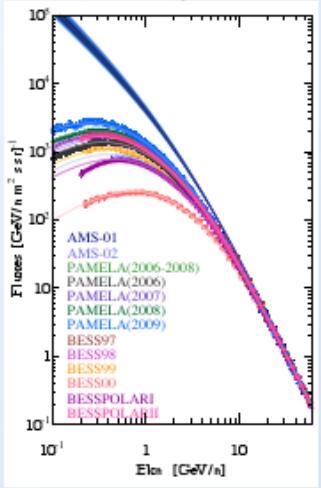

Les moniteurs à neutrons (NM)

(from A. Ghelfi)

Modélisation du signal attendu dans un NM [Dorman 2004] :

$$N(\vec{r},t) = k_{calib} \int_0^{\infty} T(R,\vec{r},t) \times \sum_{i=i_{CR}} Y_i(R,h)\, J^i_{TOA}(R,t)\, dR$$

- Taux de comptage dans le NM.
- Facteur de calibration (calculé à partir des expériences TOA).
- Fonction de transmission du champ magnétique terrestre.
- Fonction de *yield*. Modélise l'atmosphère terrestre et le NM.
- Flux TOA. Dépend de J_{IS} et ϕ.

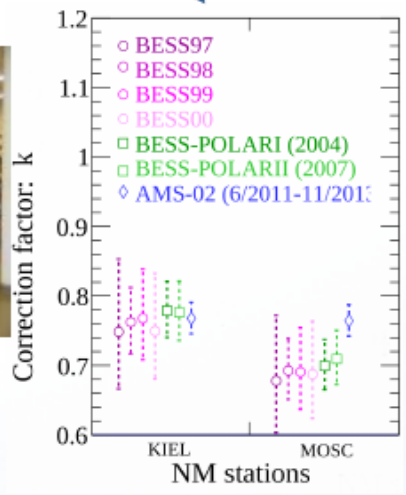

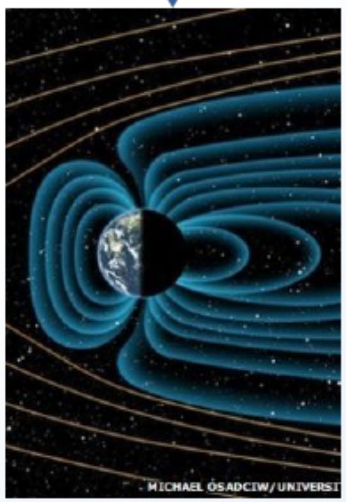

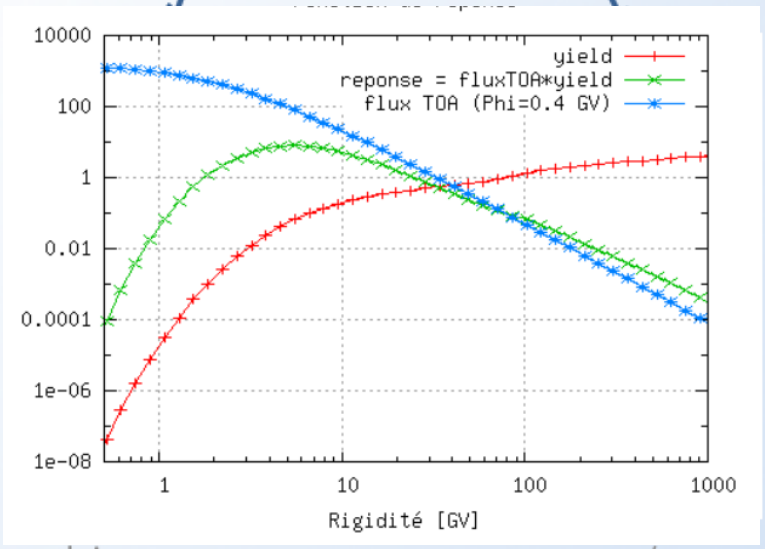

Résultats

(from A. Ghelfi)

[Ghelfi et al., 2016b]

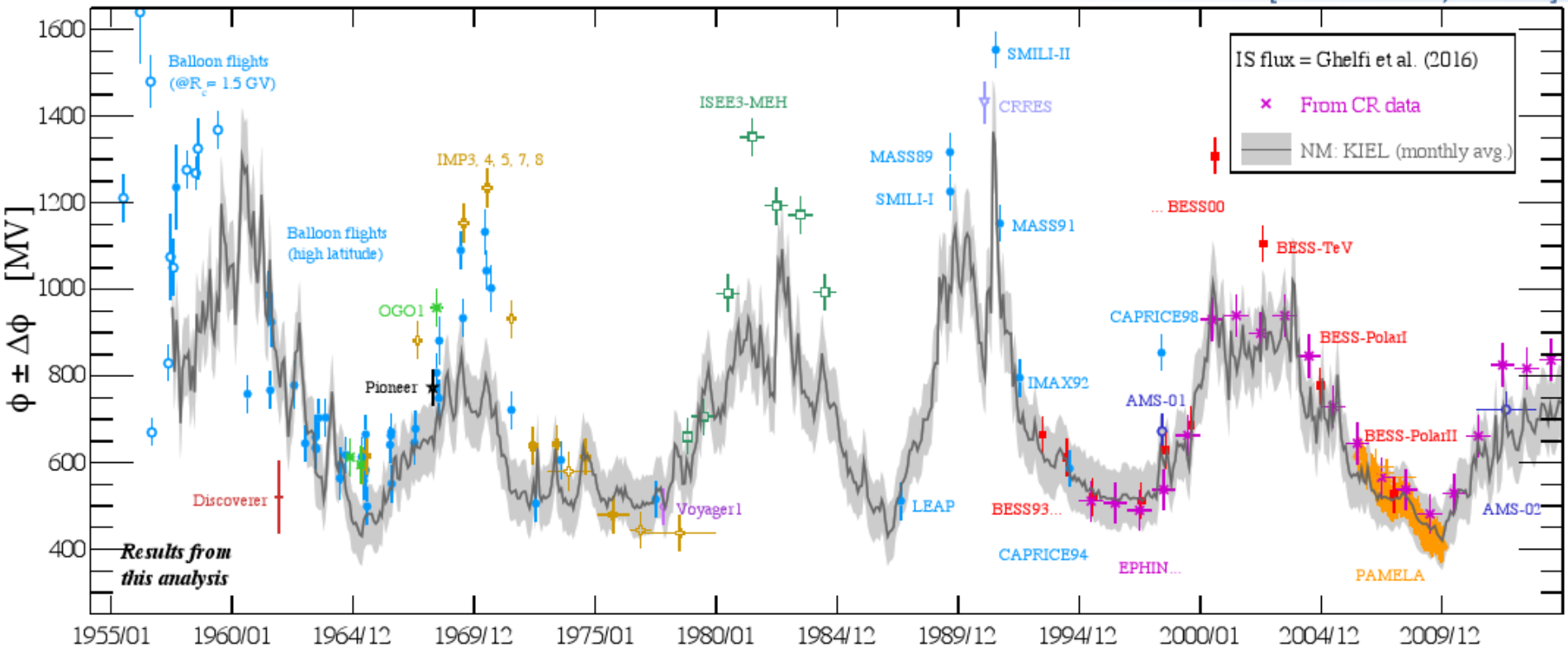

Estimation de ϕ sur 60 ans (en continu).

https://lpsc.in2p3.fr/crdb/

- Série en temps ϕ
- J_p and J_{He} pour n'importe quelle t

Différences entre NM

(from A. Ghelfi)

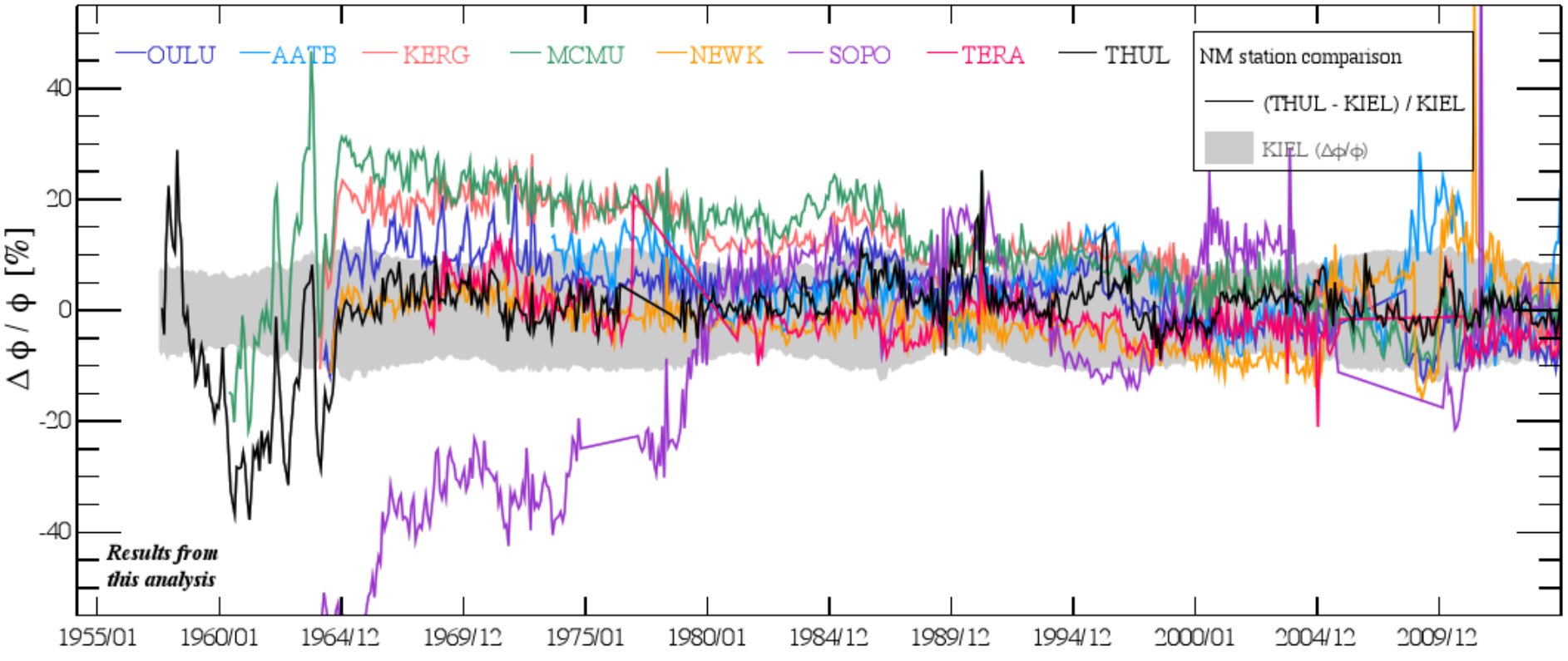

3. Count rates: Yield function uncertainties for NM64

$$N^{\mathcal{D}}(\vec{r},t) = \int_0^{\infty} \mathcal{T}(R,\vec{r},t) \times \sum_{i=\mathrm{CRs}} \mathcal{Y}_i^{\mathcal{D}}(R,h) \frac{dJ_i^{\mathrm{TOA}}}{dR}(R,t)\, dR,$$

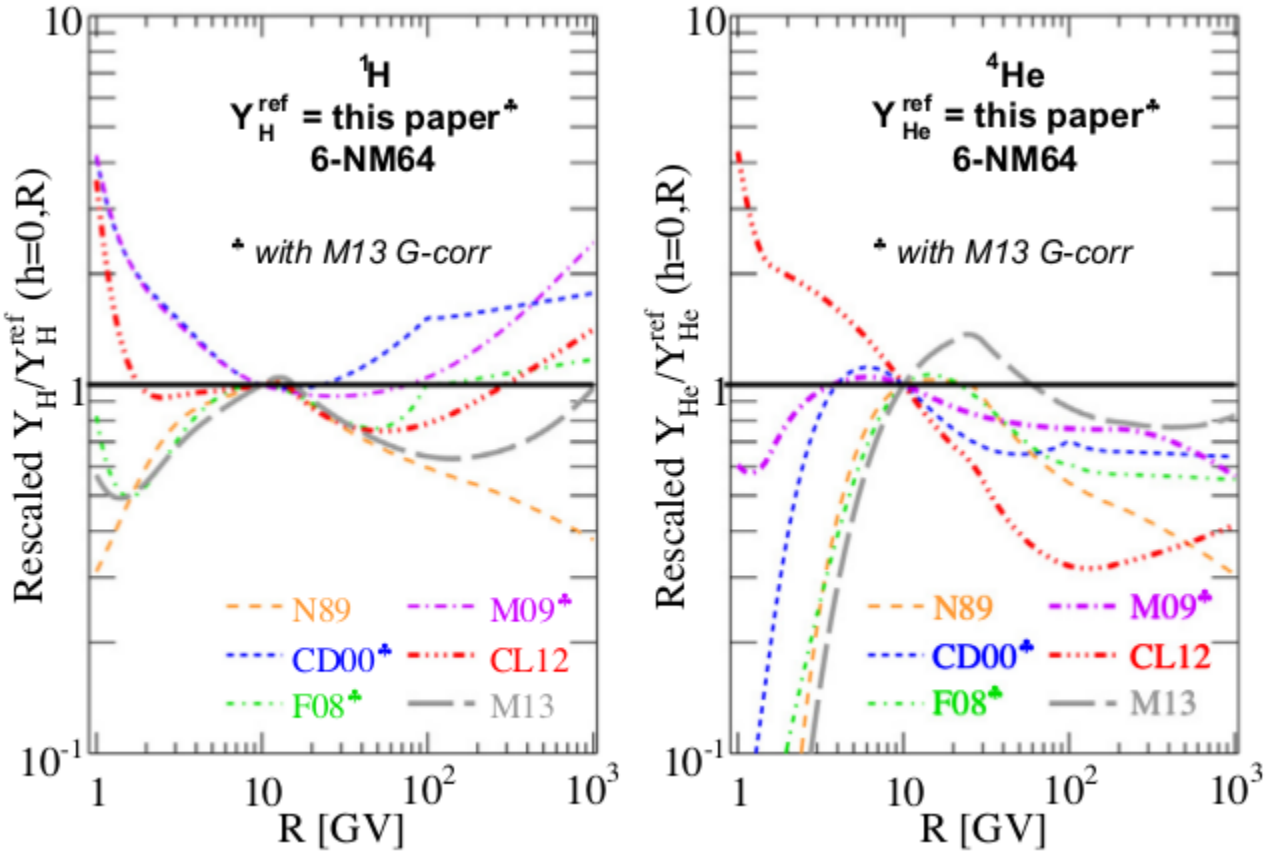

→ Large differences between various teams (R-dependent)

→ Simulations should be extended above 100 GV (important for count rates calculation

[N.B.: for MC-based yields, better results obtained with Mishev et al. (2013) correction]

Journal of Geophysical Research: Space Physics

RESEARCH ARTICLE
10.1002/2016JA022638

Special Section:
Measurement Techniques in Solar and Space Physics: Optical and Ground-Based

Monte Carlo simulation of the neutron monitor yield function

P.-S. Mangeard[1,2,3], D. Ruffolo[2], A. Sáiz[2], S. Madlee[2], and T. Nutaro[4]

[1]National Astronomical Research Institute of Thailand, Chiang Mai, Thailand, [2]Department of Physics, Faculty of Science, Mahidol University, Bangkok, Thailand, [3]Now at Department of Physics and Astronomy, University of Delaware, Newark, Delaware, USA, [4]Department of Physics, Faculty of Science, Ubon Ratchathani University, Ubon Ratchathani, Thailand

Key Points:
- We calculated the neutron monitor (NM) yield function by Monte Carlo simulation of cosmic ray-induced interactions in the atmosphere and NM
- The simulated count rate due to cosmic rays for an NM at Doi Inthanon, Thailand, matches observations to within 9%
- We calculated effects of the geomagnetic field and dead time and normalization coefficients for common NM64 detector configurations

Correspondence to:
D. Ruffolo,
david.ruf@mahidol.ac.th

Citation:
Mangeard, P.-S., D. Ruffolo, A. Sáiz, S. Madlee, and T. Nutaro (2016), Monte Carlo simulation of the neutron monitor yield function, *J. Geophys. Res. Space Physics*, *121*, 7435–7448, doi:10.1002/2016JA022638.

Abstract Neutron monitors (NMs) are ground-based detectors that measure variations of the Galactic cosmic ray flux at GV range rigidities. Differences in configuration, electronics, surroundings, and location induce systematic effects on the calculation of the yield functions of NMs worldwide. Different estimates of NM yield functions can differ by a factor of 2 or more. In this work, we present new Monte Carlo simulations to calculate NM yield functions and perform an absolute (not relative) comparison with the count rate of the Princess Sirindhorn Neutron Monitor (PSNM) at Doi Inthanon, Thailand, both for the entire monitor and for individual counter tubes. We model the atmosphere using profiles from the Global Data Assimilation System database and the Naval Research Laboratory Mass Spectrometer, Incoherent Scatter Radar Extended model. Using FLUKA software and the detailed geometry of PSNM, we calculated the PSNM yield functions for protons and alpha particles. An agreement better than 9% was achieved between the PSNM observations and the simulated count rate during the solar minimum of December 2009. The systematic effect from the electronic dead time was studied as a function of primary cosmic ray rigidity at the top of the atmosphere up to 1 TV. We show that the effect is not negligible and can reach 35% at high rigidity for a dead time >1 ms. We analyzed the response function of each counter tube at PSNM using its actual dead time, and we provide normalization coefficients between count rates for various tube configurations in the standard NM64 design that are valid to within ~1% for such stations worldwide.

1. Introduction

Neutron monitors (NMs) detect atmospheric secondary particles (SPs)—mostly neutrons—that reach the

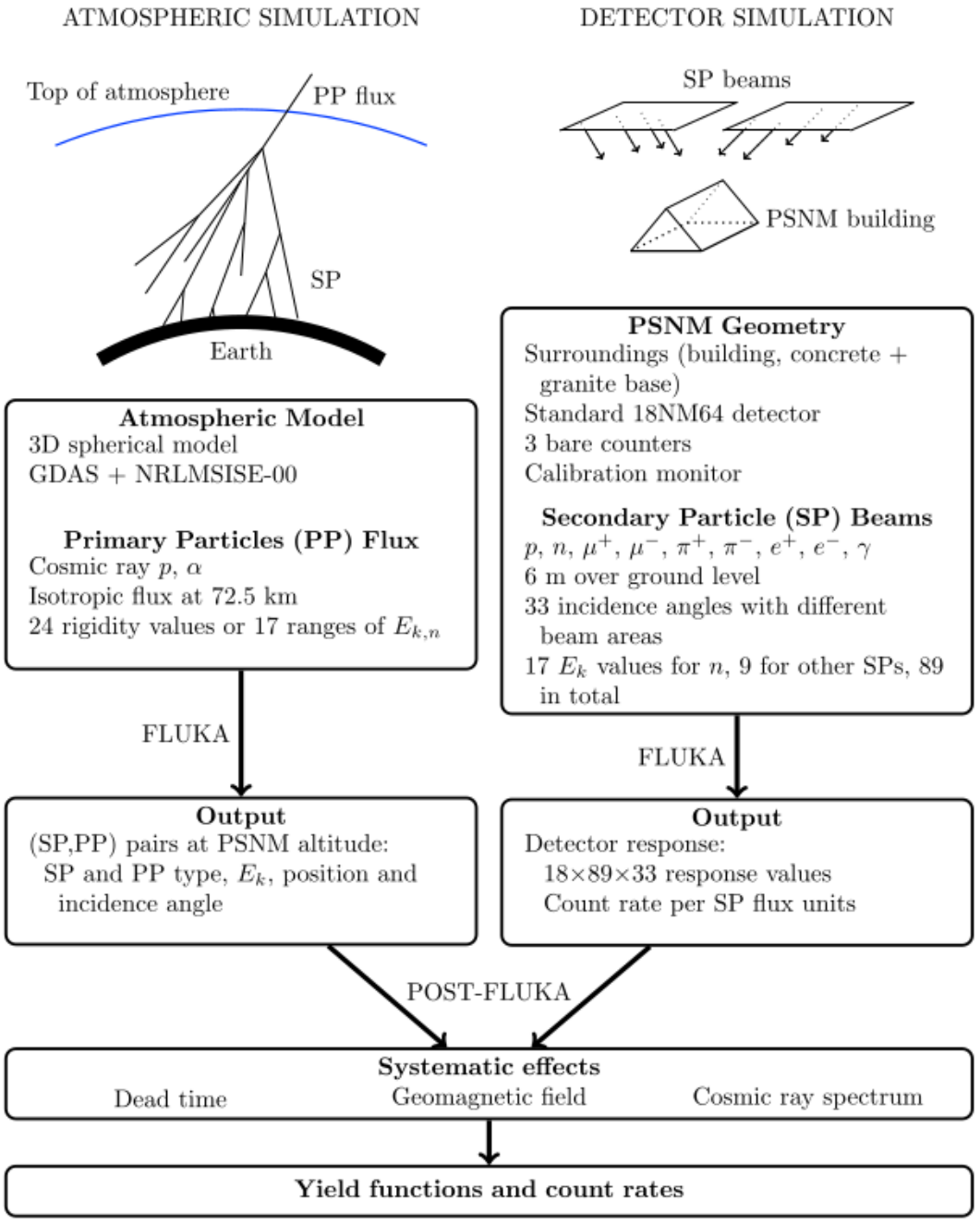

Figure 1. Methodology of Monte Carlo simulation for the Princess Sirindhorn Neutron Monitor (PSNM) at Doi Inthanon, Thailand, based on a combination of atmospheric simulation and detector simulation. See text for details.

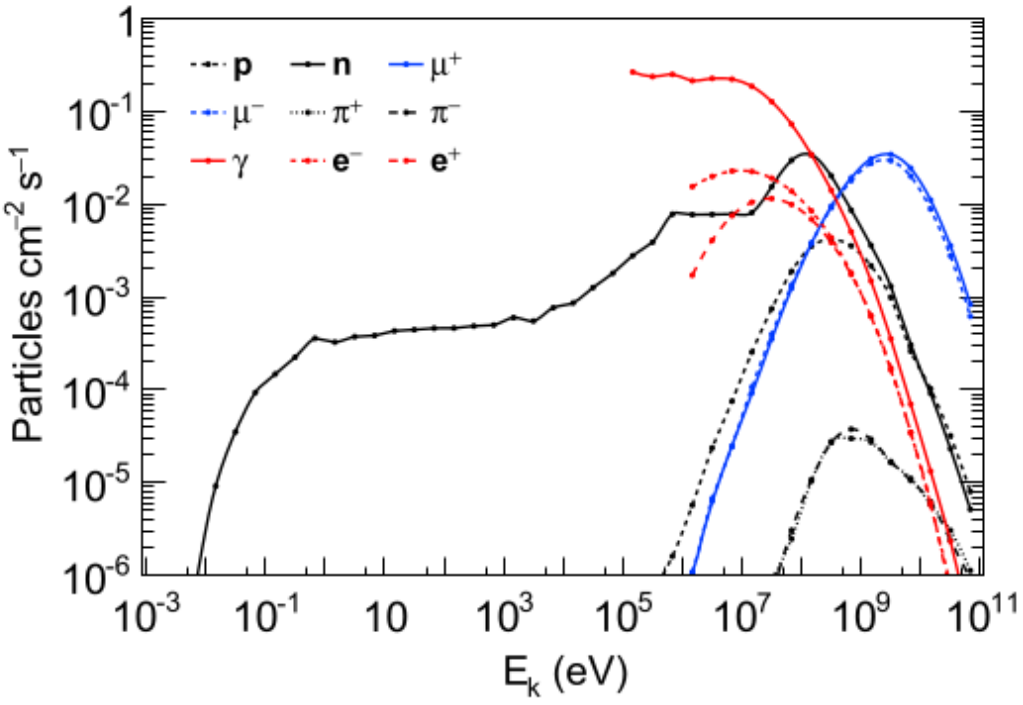

Figure 2. Simulated fluxes of various types of secondary particles at 6 m above the floor of the PSNM building from each bin in kinetic energy. Markers are plotted at the centers of bins of equal width in logarithmic scale.

The simulation of the atmospheric cascade development stops at a boundary 6 m above ground level at the altitude of the detector. The boundary is taken to be a sphere around the Earth. At the boundary, protons, neutrons, μ^+, μ^-, π^+, π^-, e^+, e^-, and γ are recorded with their characteristics and those of their parent PP. Depending on the incidence angle and the energy of the PP, the position of the SPs can spread over a large area around the latitude and longitude of the injection point. The difference of location can be larger than ~1° in both directions. Assuming spherical symmetry, each SP is translated over the boundary sphere to the detector location, and its parent PP is translated along with it. This procedure includes all SPs, taking into account the lateral extension of the atmospheric shower as well as the difference of spectrum between the core of the shower and the edge. Thus, we do not need to apply the geometric factor presented in *Mishev et al.* [2013].

In some cases we include the effect of the geomagnetic field by back tracing the antiparticle of the PP along the reversed trajectory through a model geomagnetic field. The (SP,PP) pair is rejected if the reversed anti-PP trajectory is not allowed, i.e., if it intercepts the Earth and does not connect with outer space. The International Geomagnetic Reference Field (IGRF-11) is used in this work with the techniques of *Lin et al.* [1995].

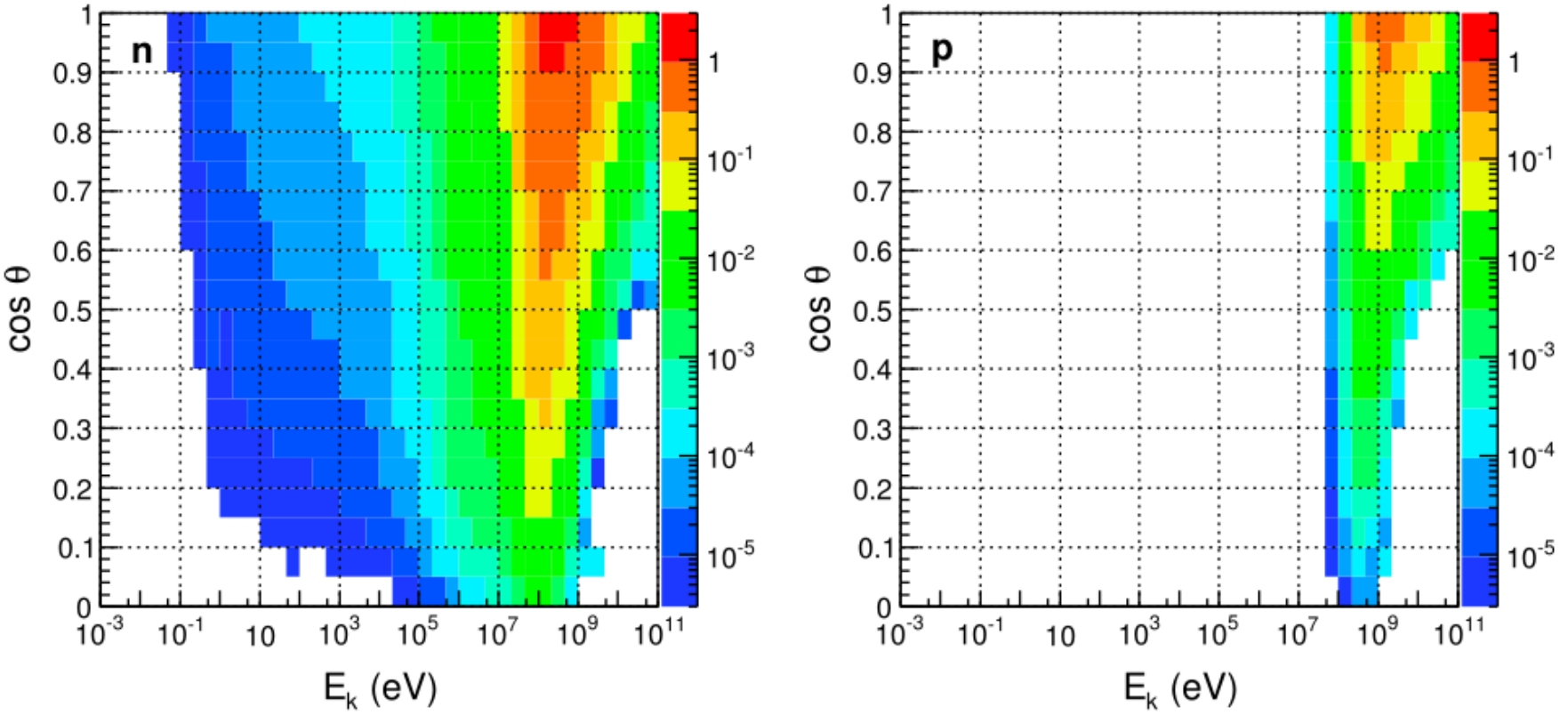

Figure 3. Simulated average count rate per tube at the PSNM due to secondary *n* (left) and *p* (right) as a function of the cosine of the zenith angle θ and of the kinetic energy E_k of the secondary particle. The palette of colors represents the average count rate per tube per bin (in Hz).

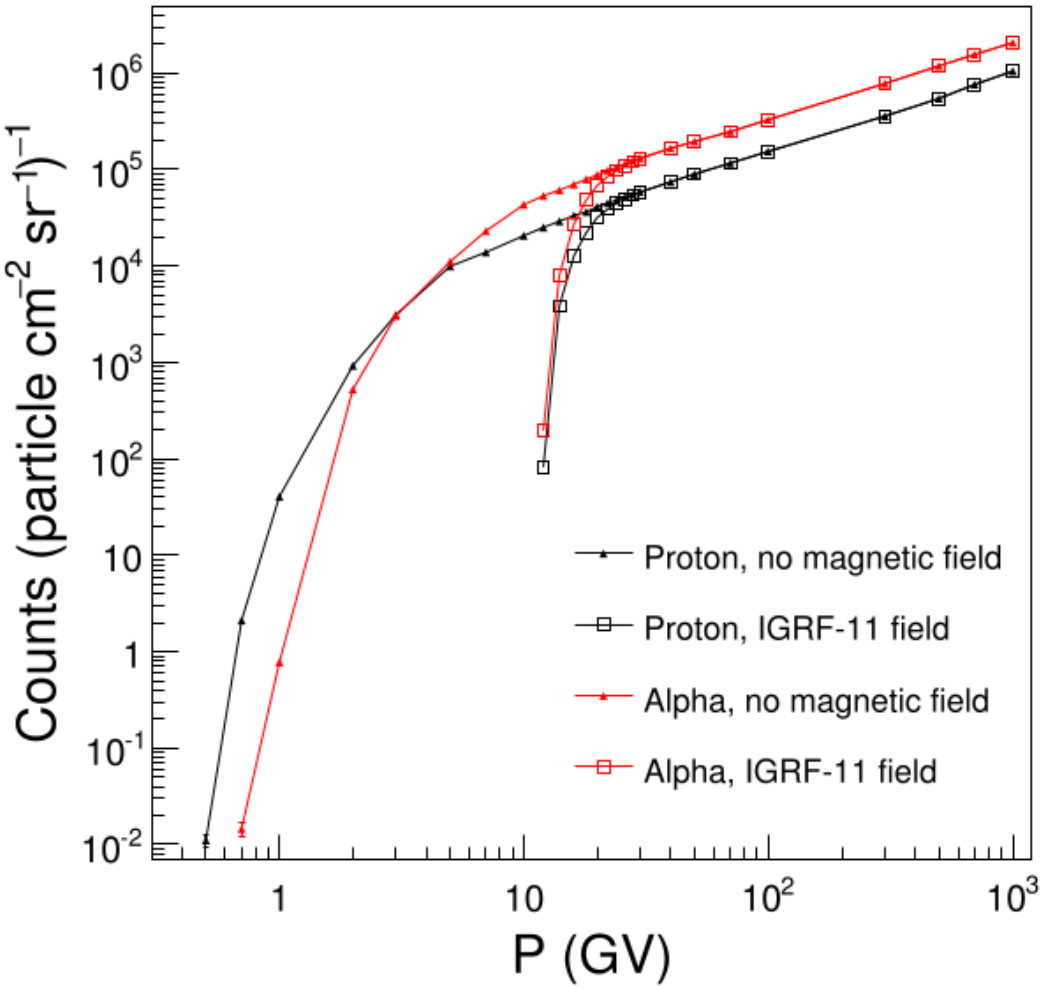

Figure 4. Calculated yield functions of the PSNM at Doi Inthanon, Thailand (altitude 2560 m), for the actual dead time. Before including the geomagnetic field, the results indicate an atmospheric cutoff at ~1 GV corresponding to the energy needed to create atmospheric secondary particles that can be detected at mountain altitude. When including the IGRF-11 model geomagnetic field, the yield function has a geomagnetic cutoff at ~17 GV.

From earlier simulations, *Aiemsa-ad et al.* [2015] showed results for the relative contributions of various SP species to the PSNM count rate. In the present simulations, about 96% of the count rate is induced by neutrons and protons. For both of these SPs, Figure 3 presents the average count rate per tube as function of the zenith angle cosine and kinetic energy of the SP. For reference, note that the total count rate per tube at PSNM is about 34 Hz. As expected, the energy range of the contributing neutrons is much broader than for the contributing protons, which also tend to produce counts at a higher energy than neutrons. We clearly see that the nonvertical incoming SPs contribute significantly to total count rate. About 21% of the total count rate is coming from neutrons with $\cos\theta < 0.7$.

3. Yield Functions

The yield functions (count rate per PP

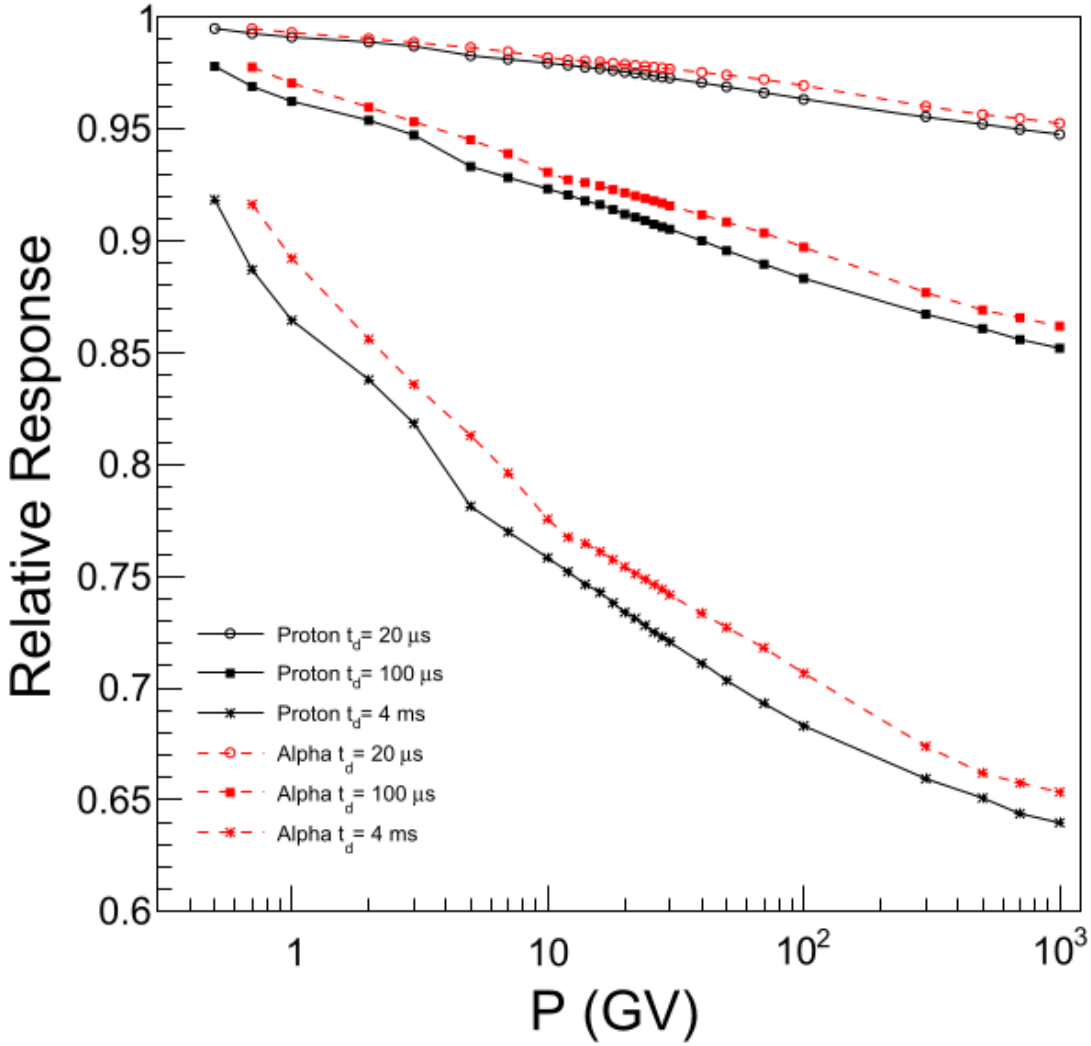

Figure 6. Relative yield functions with respect to the ideal case of no electronic dead time (t_d =0). There is a noticeable effect on the yield functions even for a typical value of t_d =20 μs.

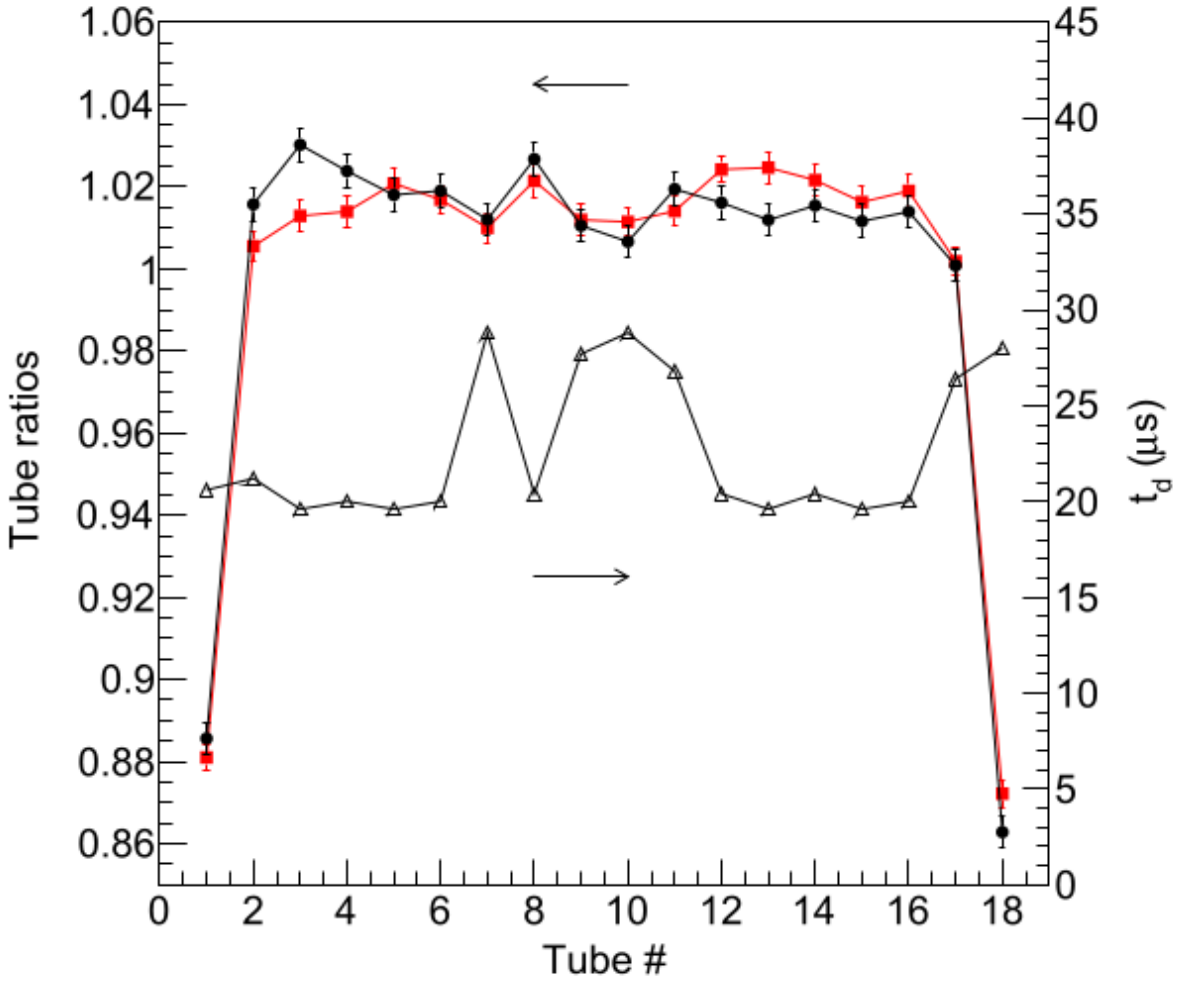

Figure 7. Count rate of each PSNM neutron counter tube relative to the tube average and measured electronic dead times. Observations are represented by filled circles. Simulated values are represented by filled squares. Dead time values are represented by open triangles. There are clear effects of the tube position relative to the edges of the row of 18 counter tubes and the dead time.